CellPress
Partner Journal

Molecular Plant
Research article

Vacuolar H$^+$-ATPase and BZR1 form a feedback loop to regulate the homeostasis of BR signaling in *Arabidopsis*

Yu-Tong Jiang[1,2,3], Lu-Han Yang[1], Ji-Xuan Zheng[4], Xian-Chen Geng[1], Yu-Xuan Bai[4], Yu-Chen Wang[4], Hong-Wei Xue[2,3] and Wen-Hui Lin[1,2,*]

[1]School of Life Sciences and Biotechnology, The Joint International Research Laboratory of Metabolic & Developmental Sciences, Shanghai Jiao Tong University, Shanghai 200240, China

[2]Shanghai Collaborative Innovation Center of Agri-Seeds, Joint Center for Single Cell Biology, Shanghai 200240, China

[3]School of Agriculture and Biology, Shanghai Jiao Tong University, Shanghai 200240, China

[4]Zhiyuan College, Shanghai Jiao Tong University, Shanghai 200240, China

***Correspondence: Wen-Hui Lin (whlin@sjtu.edu.cn)**

https://doi.org/10.1016/j.molp.2023.10.007

ABSTRACT

Brassinosteroid (BR) is a vital plant hormone that regulates plant growth and development. BRASSINAZOLE RESISTANT 1 (BZR1) is a key transcription factor in BR signaling, and its nucleocytoplasmic localization is crucial for BR signaling. However, the mechanisms that regulate BZR1 nucleocytoplasmic distribution and thus the homeostasis of BR signaling remain largely unclear. The vacuole is the largest organelle in mature plant cells and plays a key role in maintenance of cellular pH, storage of intracellular substances, and transport of ions. In this study, we uncovered a novel mechanism of BR signaling homeostasis regulated by the vacuolar H$^+$-ATPase (V-ATPase) and BZR1 feedback loop. Our results revealed that the *vha-a2 vha-a3* mutant (*vha2*, lacking V-ATPase activity) exhibits enhanced BR signaling with increased total amount of BZR1, nuclear-localized BZR1, and the ratio of BZR1/phosphorylated BZR1 in the nucleus. Further biochemical assays revealed that VHA-a2 and VHA-a3 of V-ATPase interact with the BZR1 protein through a domain that is conserved across multiple species. VHA-a2 and VHA-a3 negatively regulate BR signaling by interacting with BZR1 and promoting its retention in the tonoplast. Interestingly, a series of molecular analyses demonstrated that nuclear-localized BZR1 could bind directly to specific motifs in the promoters of VHA-a2 and VHA-a3 to promote their expression. Taken together, these results suggest that V-ATPase and BZR1 may form a feedback regulatory loop to maintain the homeostasis of BR signaling in *Arabidopsis*, providing new insights into vacuole-mediated regulation of hormone signaling.

Key words: BR, BZR1, vacuole, V-ATPase, tonoplast

Jiang Y.-T., Yang L.-H., Zheng J.-X., Geng X.-C., Bai Y.-X., Wang Y.-C., Xue H.-W., and Lin W.-H. (2023). Vacuolar H$^+$-ATPase and BZR1 form a feedback loop to regulate the homeostasis of BR signaling in *Arabidopsis*. Mol. Plant. **16**, 1976–1989.

INTRODUCTION

Brassinosteroid (BR) is an essential plant hormone that regulates plant growth and development. BR rarely travels over long distances (Vukašinović and Russinova, 2018), so BR signaling in local tissues is particularly important. BR signal transduction must cross two physical barriers, the plasma membrane, which separates intracellular components from the extracellular matrix, and the nuclear envelope, which separates genetic materials from the cytosolic contents (Contrò et al., 2015; Levin, 2015). On the plasma membrane, BR signaling is activated and transcription factors such as BRASSINAZOLE RESISTANT 1 (BZR1) can be dephosphorylated and accumulate in the nucleus, where they activate or repress the transcription of their downstream target genes (He et al., 2005). Thus, the localization of BZR1 is crucial for BR signaling. BR promotes BZR1 nuclear accumulation by inactivating BRASSINOSTEROID INSENSITIVE 2 (BIN2) and inhibiting the 14-3-3-induced nuclear export and degradation of phosphorylated BZR1 (Wang et al., 2021). Recent studies

Published by the Molecular Plant Shanghai Editorial Office in association with Cell Press, an imprint of Elsevier Inc., on behalf of CSPB and CEMPS, CAS.

have revealed that auxin also promotes BZR1 nuclear accumulation by inhibiting the stability of 14-3-3 proteins (Yu et al., 2023). However, whether BZR1 has a positioning anchor in the cytoplasm before nuclear entry is unclear (Wang et al., 2021), and this prompted us to explore the dynamic subcellular localization of BZR1 in more detail.

Signal transduction in plants requires synergistic work between the endomembrane system and organelles. Vacuoles are the largest organelle in mature plant cells and play essential roles in plant growth and development. Vacuoles maintain turgor pressure, regulate cellular acidity, and store substances in plant cells (Marty, 1999). Furthermore, vacuoles are an integral part of the endomembrane system and control the transport and localization of key proteins through endocytosis and degradation pathways (Martinoia et al., 2007). The plant cell plasma membrane is surrounded by a rigid cell wall and therefore has less fluidity than animal cell membranes. The tonoplast (vacuolar membrane) has more capacity to move than the plasma membrane in plant cells, and tonoplast proteins have important roles in intracellular protein trafficking. Transport across the tonoplast is energized by two proton pumps, the vacuolar H^+-ATPase (V-ATPase) and the vacuolar H^+-pyrophosphatase (V-PPase) (Hedrich et al., 1989). V-PPase is a homodimer of a single polypeptide, whereas V-ATPase is a multi-subunit proton pump consisting of two subcomplexes (Maeshima, 2000; Martinoia et al., 2007). The peripheral V_1 complex (VHA-A to VHA-H) of V-ATPase is responsible for ATP hydrolysis, whereas the membrane-integral V_0 complex (VHA-a, -c, -c′, -c″, -d, and -e) is in charge of proton translocation from the cytosol into the vacuole (Maeshima, 2000; Gaxiola et al., 2007; Cipriano et al., 2008). The VHA-a subunit is the largest V-ATPase subunit and has multiple isoforms, each of which mediates the differential targeting of V-ATPase to specific organelles (Zhao et al., 2015; Vasanthakumar et al., 2019). Among these isoforms, the a2 and a3 subunits (encoded by *VHA-a2* and *VHA-a3*) are crucial for specific targeting to the vacuole and assembly of V-ATPase in *Arabidopsis thaliana* (*Arabidopsis*) (Dettmer et al., 2006). H^+-ATPase plays an important role in plant hormone signal transduction. Auxin activates the plasma membrane-localized H^+-ATPase through specific phosphorylation of TMK family proteins to promote cell elongation and tissue growth (Lin et al., 2021). Recent analyses of vacuoles and tonoplast proton pumps have indicated that vacuole-related pathways play a key role in the signal transduction of auxin, cytokinin, abscisic acid, and other plant hormones (Burla et al., 2013; Ranocha et al., 2013; Jiskrová et al., 2016; Liu et al., 2018). The weak V-ATPase mutant *deetiolated3* (*det3*) has altered BR sensitivity due to reduced Golgi and *trans*-Golgi network/early endosome motility (Luo et al., 2015). However, whether V-ATPase directly regulates BR signaling and BZR localization through the vacuole-related pathway remains unclear. In addition, V-ATPase regulates protein transport in animal cells (Hiesinger et al., 2005; Marshansky et al., 2014), and it remains to be investigated whether tonoplast V-ATPase has a similar role in plants. Thus, given the importance of BZR1 subcellular localization and the conserved function of V-ATPase among species, it is worth studying how V-ATPase is involved in BZR1 cytoplasmic retention and BR signaling.

RESULTS

BR signaling is activated in mutants that lack tonoplast V-ATPase activity

Here, we report the phenotype of the *vha-a2 vha-a3* mutant (*vha2*, lacking the a subunits—VHA-a2 and VHA-a3—of V-ATPase) to explore the relationship between vacuole-localized V-ATPase and BR signaling. We tested the BR sensitivity of *vha2* mutant seedlings using exogenous application of naturally occurring epibrassinolide (eBL) (Figure 1A). We observed that the *vha2* seedlings were more sensitive to increasing eBL concentrations, as measured by root growth of light-grown seedlings. The highest eBL concentration that promoted root growth was lower in the mutant than in Columbia-0 (Col) (Figure 1A). We also used real-time quantitative PCR (qRT–PCR) to measure the expression of two BR biosynthesis genes negatively regulated by BR, *CONSTITUTIVE PHOTOMORPHOGENIC DWARF* (*CPD*) and *DWARF 4* (*DWF4*), in *vha2* (Sun et al., 2010). *CPD* and *DWF4* expression was downregulated in *vha2* seedlings compared with Col (Figure 1B). BR signaling influences chloroplast ultrastructure, and mutants with higher BR signaling have fewer thylakoid lamellae (Zhang et al., 2021). We therefore examined chloroplast ultrastructure and established that *vha2* cotyledons had significantly fewer thylakoid lamellae than those of Col (Figure 1C and 1D), suggesting that *vha2* has higher BR signaling in *vivo*. BR plays a key role in the skotomorphogenesis of seedlings, and RNA sequencing (RNA-seq) of dark-grown hypocotyls is a widely used approach in BR-related studies (Sun et al., 2010). To further examine the association of VHA-a2 and VHA-a3 with the BR pathway, we performed RNA-seq on hypocotyls of etiolated *vha2* and Col seedlings. There were 3303 differentially expressed genes (DEGs) out of 23269 genes in *vha2* compared with Col (Supplemental Figure 1A and 1B). Kyoto Encyclopedia of Genes and Genomes (KEGG) analysis of these DEGs revealed enrichment in pathways including plant hormone signal transduction, ribosome, and BR biosynthesis (Figure 1E). Expression of *VHA-a2* and *VHA-a3* was significantly lower in *vha2* than in Col (Figure 1F), supporting the reliability of the RNA-seq data. KEGG analysis revealed a high ratio of DEGs associated with BR biosynthesis (Figure 1E). Downregulated DEGs associated with BR biosynthesis in *vha2* included *CPD*, *DWF4*, *ROTUNDIFOLIA 3* (*ROT3*), and *BRASSINOSTEROID-6-OXIDASE 2* (*BR6OX2*), which are known to be negatively regulated by BR (Figure 1F) (Sun et al., 2010). We performed a separate gene ontology analysis of hormone-related DEGs, and the results showed that BR-related pathways dominated (Supplemental Figure 1C). Compared with DEGs in BR-treated Col or BR-signal-enhanced mutants (Goda et al., 2004; Sun et al., 2010; Nolan et al., 2023), DEGs in *vha2* included many known genes involved in the BR response (Supplemental Figure 2). The above results imply that BR signaling is increased in *vha2*.

To investigate the mechanism underlying the increased BR signaling in *vha2*, we assessed the abundance of the BR receptors BRASSINOSTEROID INSENSITIVE 1 (BRI1) and BRI1-ASSOCIATED KINASE 1 (BAK1) in *vha2*, *bzr1-1D* (a signaling-enhanced mutant), and *bri1-301* (a loss-of-function mutant) (Kinoshita et al., 2005; Wang et al., 2005; Wang and Chory, 2006; Ji et al., 2011). Although we observed changes in BRI1 and BAK1

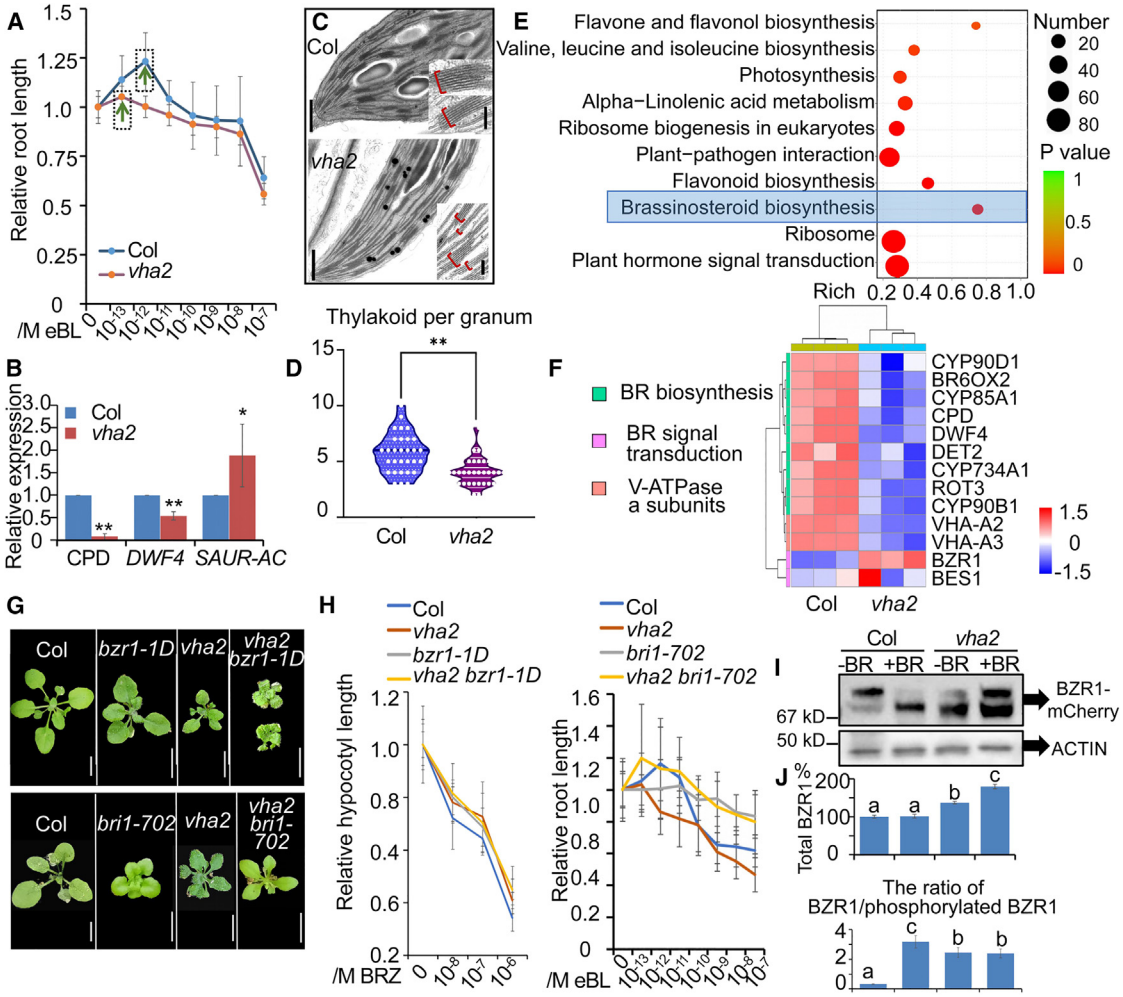

Figure 1. V-ATPase-deficient mutant *vha2* has activated BR signaling.

(A) Relative root length of 5-DAG light-grown seedlings of Col and *vha2* treated with different concentrations of eBL. Green arrows indicate the highest eBL concentration to promote root elongation. Bars represent the mean ± SD (n = 15).

(B) Transcript levels of *CPD*, *DWF4*, and *SAUR-AC* in 5-DAG light-grown seedlings of Col and *vha2*. Error bars represent confidence intervals (CIs) calculated from three biological replicates (each biological replicate was composed of three technical replicates) of each sample in the qRT–PCR assay. Asterisks indicate significant differences compared with the respective WT control (Student's t-test; $^{*}p < 0.05$, $^{**}p < 0.01$).

(C) Thylakoid ultrastructure of cotyledons in 8-DAG seedlings of Col and *vha2*. Scale bars represent 1 μm (main image) and 200 nm (magnified image).

(D) Statistical analysis of grana stacking in the mesophyll chloroplasts in **(A)**. Data are mean ± SD (n = 15). Asterisks indicate significant differences compared with the respective Col WT control (Student's t-test; $^{*}p < 0.05$, $^{**}p < 0.01$).

(E) KEGG pathway analysis of differentially expressed genes (DEGs) (*vha2* versus Col) in the transcriptome analysis.

(F) DEGs in BR-related pathways and V-ATPase a subunits in *vha2*. Red and blue indicate upregulation and downregulation, respectively.

(G) Phenotypic analysis of 20-DAG *vha2 bzr1-1D* and *vha2 bri1-702* compared with the parent mutants and WT control. Scale bars represent 1 cm.

(H) Relative hypocotyl lengths of 5-DAG dark-grown seedlings of the *vha2 bzr1-1D* mutant, parent mutants, and WT control treated with different concentrations of BRZ (left), and relative root lengths of 5-DAG light-grown seedlings of the *vha2 bzr1-1D mutant, parent mutants, and WT control* treated with different concentrations of eBL (right). Bars represent the mean ± SD (n = 15).

(I) Western blot analysis of BZR1 protein in Col and *vha2* using the anti-mCherry antibody. 5-DAG light-grown seedlings were treated with (+BR) or without (−BR) 1 μM eBL for 30 min before western blot assays.

(J) Semi-quantitative analysis of total BZR1 protein and the BZR1/phosphorylated BZR1 ratio detected in **(I)**. Error bars represent the mean ± SD (n = 3). Lowercase letters indicate significant differences among different materials (one-way ANOVA, $p < 0.05$).

levels in *vha2* relative to Col, they were not as obvious as those in *bzr1-1D* and *bri1-301* (Supplemental Figure 3A), suggesting that increased BR signaling in *vha2* is not strongly associated with a greater abundance of BR receptors, consistent with a previous report (Luo et al., 2015). After BR signaling is activated, the activity of downstream transcription factors that control BR signaling is enhanced in plant cells. The BZR1–BRI1 EMS-SUPPRESSOR 1 (BZR/BES) family is a class of BR-related transcription factors that are routinely used to assess BR signaling phenotypes, especially BZR1 and BES1 (He et al., 2005; Li and Deng, 2005). Immunoblot analysis revealed that the ratio of nuclear-localized BES1 and phosphorylated BES1 was similar in *vha2* and Col seedlings (Supplemental Figure 3B and 3C), and BZR1 is essential in mediating BR-regulated gene expression (Figure 1I).

RNA-seq also revealed that BZR1 expression was significantly upregulated in *vha2* compared with Col, whereas there was no significant difference in BES1 expression (Figure 1F). However, an association of BZR1 protein with V-ATPase has rarely been reported. We therefore crossed *vha2* with *bzr1-1D* and *bri1-702* (a loss-of-function mutant). Compared with *vha2* and *bzr1-1D*, *vha2 bzr1-1D* plants had a more severe BR-signaling-enhanced phenotype, including curled leaves and roots (Figure 1G; Supplemental Figure 3D and 3E). Furthermore, under BRZ treatment, *vha2* was strongly resistant to BRZ, indicating that BR signaling in *vha2* was very high. It may be difficult to measure higher BR signaling in *vha2 bzr1-1D* under BRZ treatment compared with *vha2* and *bzr1-1D* (Figure 1H). The shape and petiole of *vha2 bri1-702* rosette leaves more closely resembled those of Col compared with *bri1-702* (Figure 1G). Light-grown *vha2 bri1-702* seedlings showed greater sensitivity to eBL treatment compared with *bri1-702* (Figure 1H). We also used qRT–PCR to measure expression of *CPD* and *DWF4* in *vha2 bzr1-1D* and *vha2 bri1-702*. *CPD* expression was downregulated in *vha2 bzr1-1D* seedlings compared with *bzr1-1D*, and *CPD* and *DWF4* expression was downregulated in *vha2 bri1-702* seedlings compared with *bri1-702* (Supplemental Figure 3F). qRT–PCR assays of *vha2 bzr1-1D* seedlings also demonstrated higher BR signaling in *vha2 bzr1-1D* (Supplemental Figure 3E) than in *vha2* and *bzr1-1D*. These results suggest that higher BR signaling in *vha2* partially rescued the suppression of BR signaling in *bri1-702*. We next crossed *vha2* to *bin2-1* (a gain-of-function mutant of BIN2 with suppressed BR signaling). Because the growth and fertility of homozygous *bin2-1* mutants are very poor, experiments involving the *bin2-1* mutant in this research mainly used heterozygous mutants, *bin2-1*$^{+/-}$ (Li et al., 2001). The growth status of *vha2 bin2-1*$^{+/-}$ (*vha-a2-/vha-a2-vha-a3-/vha-a3-*, *bin2-1/BIN2*) was much better than that of *bin2-1*$^{+/-}$ (taller inflorescence axis), and *DWF4* expression was downregulated in *vha2 bin2-1*$^{+/-}$ seedlings compared with *bin2-1*$^{+/-}$ (Supplemental Figure 3G and 3H). These results suggest that BR signaling is increased in *vha2* and that vacuole-localized V-ATPase is involved in BR signaling.

Based on the results above, we focused on BZR1 to investigate the association between V-ATPase and BR signaling. When BR is increased, BR signaling is activated, and BZR1 accumulates in the nucleus following dephosphorylation (Tang et al., 2011; Wang et al., 2016, 2021). We therefore examined the total amount and phosphorylation level of BZR1 in *vha2*. Immunoblot analysis showed that the total amount of BZR1 and the ratio of BZR1 to phosphorylated BZR1 was significantly higher in *vha2* seedlings compared with Col, consistent with the BR-signal-enhanced phenotypes observed in *vha2* (Figure 1I and 1J). There were no significant differences in the BZR1 phosphorylation level of *vha2*, with or without BR treatment, demonstrating that *vha2* already had high BR signaling and might not be more sensitive to BR treatment.

V-ATPase regulates the nucleocytoplasmic localization of BZR1

To determine whether the subcellular localization of BZR1 was altered in *vha2*, we performed a nucleocytoplasmic separation experiment using light-grown seedlings of Col and *vha2* 5 days after germination (DAG). Immunoblot analysis revealed that *vha2* accumulated more nuclear-localized BZR1, with a higher BZR1/phosphorylated BZR1 ratio compared with Col (Figure 2A–2C). These results suggested that light-grown *vha2* seedlings have higher BR signaling than Col. We also performed a nucleocytoplasmic separation experiment using 5-DAG dark-grown seedlings (Supplemental Figure 4A–4C) and rosette leaves from 35-DAG light-grown plants (Supplemental Figure 4D and 4E). The results of these assays were generally consistent with those of light-grown seedlings. Overall, there was more nuclear-localized BZR1 and a higher nuclear BZR1/phosphorylated BZR1 ratio in *vha2* than in Col.

To further confirm the effect of V-ATPase on BZR1 localization, we characterized the fluorescence distribution pattern of a BZR1-YFP (yellow fluorescent protein) fusion protein encoded by *pBZR1:BZR1-YFP* in Col with or without BR treatment and in *vha2*. Confocal microscopy and fluorescence quantification revealed that the total abundance of BZR1-YFP was significantly higher in *vha2* than in Col (Figure 2D–2F). BZR1-YFP constitutively localized to the nucleus in *vha2* and Col with BR treatment (Figure 2D–2F). By contrast, a substantial amount of BZR1-YFP localized to the cytosol in Col without BR treatment (Figure 2D–2F). These results revealed that deficiency in the vacuole-localized V-ATPase increases the total amount of BZR1 and promotes BZR1 accumulation in the nucleus, a pattern similar to that observed when Col is treated with BR.

To determine whether vacuole-localized V-ATPase directly affects BZR1 localization, we purified vacuoles from the *pBZR1:BZR1-YFP pSYP22:SYP22-RFP* transgenic line. Confocal microscopy revealed that cytoplasmic BZR1 could localize to the tonoplast, as evidenced by overlapping fluorescence of BZR1-YFP and SYP22-RFP (red fluorescent protein) on the tonoplast (Figure 2G–2I). By contrast, the overlap coefficient of tonoplast BZR1-YFP and SYP22-RFP was lower in *vha2* compared with that in Col, and this tendency was consistent with vacuoles of BR-treated Col (Figure 2G–2I). Taken together, these results indicate that BZR1 partially localizes to the tonoplast in wild-type (WT) cells and that both total and nuclear-localized BZR1 are higher in *vha2*.

V-ATPase interacts with BZR1 through a domain that is conserved in multiple species

To further investigate the relationship between V-ATPase and BZR1, we generated transgenic plants harboring *pVHA-a3:VHA-a3-GFP* (encoding the VHA-a3 subunit of V-ATPase fused to the green fluorescent protein [GFP]) and *pBZR1:BZR1-mCherry* (encoding a fusion between BZR1 and the mCherry). Confocal microscopy revealed that VHA-a3-GFP co-localized with BZR1-mCherry in *Arabidopsis* roots, and transient co-transformation of the *pUBQ10:VHA-a2-GFP* or *pUBQ10:VHA-a3-GFP* construct with *pUBQ10:BZR1-mCherry* in *Nicotiana benthamiana* leaves confirmed this result (Supplemental Figure 5A and 5B).

Next, we explored how V-ATPase might affect the subcellular localization of BZR1. Given that V-ATPase modulates the subcellular localization of BZR1 and that VHA-a2 and VHA-a3 partially co-localize with BZR1 at the tonoplast, we hypothesized that BZR1 might interact with VHA-a2 and VHA-a3. To determine whether BZR1 and/or its regulatory proteins interact with the VHA-a2 and VHA-a3 subunits (Ryu et al., 2007; Tang et al., 2011), we

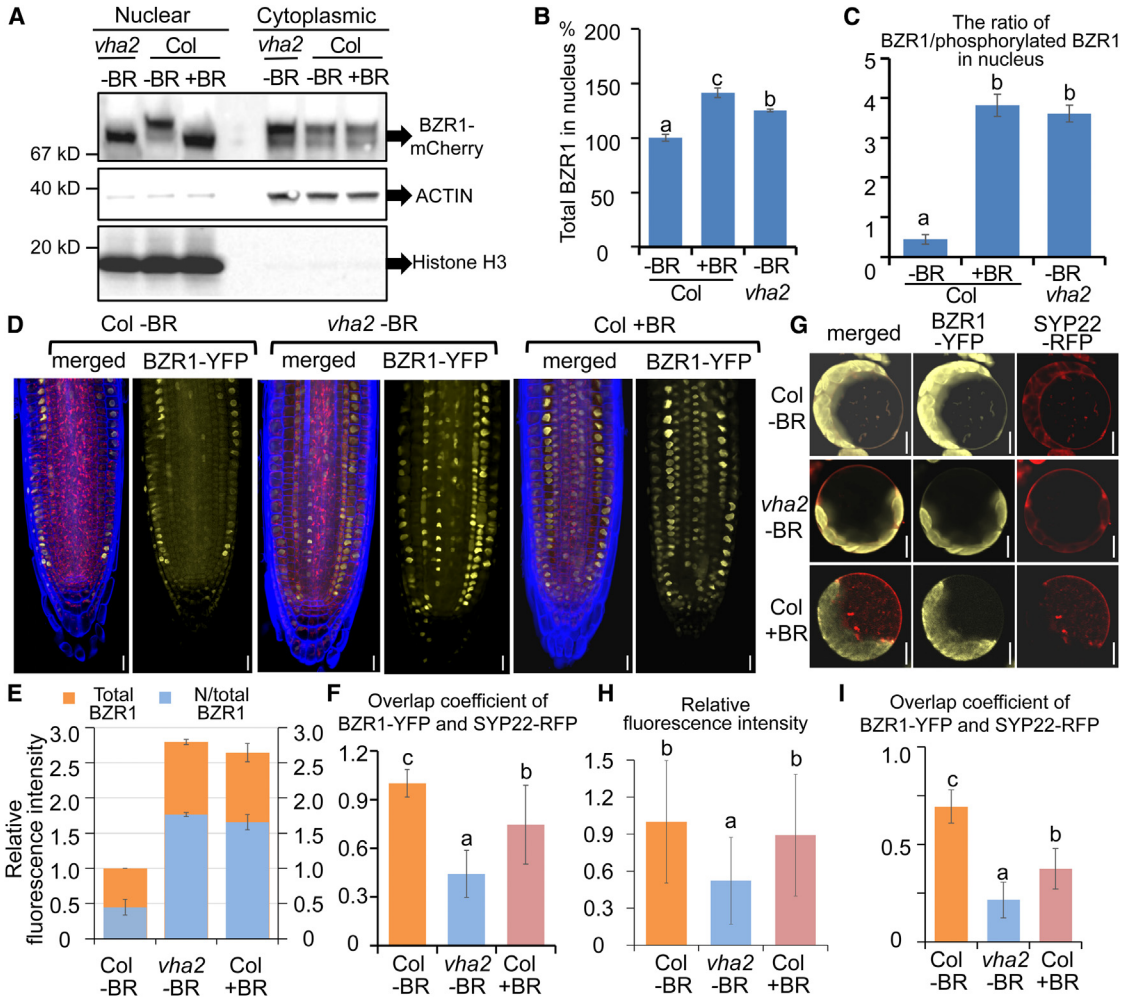

Figure 2. V-ATPase regulates the subcellular localization of BZR1 protein.

(A) Nucleocytoplasmic protein separation analysis of BZR1 protein in Col and *vha2* using the anti-mCherry antibody. 5-DAG light-grown seedlings were treated with (+BR) or without (−BR) 1 μM eBL for 30 min before western blot assays.

(B) Semi-quantitative analysis of total BZR1 protein detected in **(A)**. Error bars represent the mean ± SD (n = 3). Lowercase letters indicate statistically significant differences among different materials (one-way ANOVA, $p < 0.05$).

(C) Nuclear BZR1/phosphorylated BZR1 ratio detected in **(A)**. Error bars represent the mean ± SD (n = 3). Lowercase letters indicate statistically significant differences among different materials (one-way ANOVA, $p < 0.05$).

(D) Confocal microscopy examination of the subcellular localization of BZR1-YFP. 5-DAG light-grown seedlings were treated with (+BR) or without (−BR) 1 μM eBL for 30 min and then visualized. Scale bars represent 20 μm.

(E) Ratio of nuclear-localized/total BZR1-YFP quantified by fluorescence levels in **(D)**. Error bars represent the mean ± SD (15 cells from 3 roots were measured separately).

(F) Semi-quantitative analysis of the overlap coefficient of BZR1-YFP and SYP22-RFP. Relative fluorescence signal data were extracted from normalized mean gray levels in **(D)**. Error bars represent the mean ± SD of three biological replicates (15 cells from 3 roots were measured separately). Lowercase letters indicate statistically significant differences among different materials (one-way ANOVA, $p < 0.05$).

(G) Confocal microscopy examination of tonoplast BZR1-YFP and SYP22-RFP in vacuoles from 20-DAG light-grown plants. Leaves from 20-DAG soil-grown plants were cut and treated with 1 μM eBL (+BR) or 1 μM BRZ (−BR) for 30 min and then examined (n = 15). Scale bars represent 10 μm.

(H) Total fluorescence signal of BZR1-YFP detected in **(G)**. Error bars represent the mean ± SD (n = 15). Lowercase letters indicate statistically significant differences among different materials (one-way ANOVA, $p < 0.05$).

(I) Semi-quantitative analysis of the overlap coefficient of BZR1-YFP and SYP22-RFP. Relative fluorescence signal data were extracted from normalized mean gray levels in **(G)**. Bars represent the mean ± SD of three biological replicates (n = 15). Lowercase letters indicate statistically significant differences among different materials (one-way ANOVA, $p < 0.05$).

performed bimolecular fluorescence complementation (BiFC) assays in *N. benthamiana* cells. We observed that BZR1, PROTEIN PHOSPHATASE 2A regulatory subunits (PP2A-B′-α and PP2A-B′-β), and the GENERAL GROWTH REGULATOR 14-3-3 proteins (GRF6 and GRF10) physically interacted with VHA-a2 and VHA-a3 (Supplemental Figure 6A). We also examined the expression of BZR1S173A (14-3-3-binding-deficient form), BZR1ΔPEST (PP2A-binding-deficient form), and BZR1TTTT (without nuclear localization signals) in the *vha2* background (Wang et al., 2021). The results showed that VHA-a2 and VHA-a3

interacted with PP2A subunits and 14-3-3 proteins, but the expression of BZR1S173A, BZR1ΔPEST, and BZR1TTTT in the *vha2* background did not differ significantly from that in Col (Supplemental Figure 6), suggesting that the regulation of BZR1 by VHA-a2 and VHA-a3 might not be directly linked to the 14-3-3- or PP2A-associated pathways. It has been reported that BZR1 degradation (when released from 14-3-3 proteins) and dephosphorylation (by PP2As) occur mainly in the nucleus (Wang et al., 2021). Because VHA-a2 and VHA-a3 are localized in the tonoplast, we focused on the interactions of VHA-a2 and VHA-a3 with BZR1 rather than PP2A or GRFs. Accordingly, we performed co-immunoprecipitation (co-IP) assays in transgenic lines harboring *pVHA-a3*:*VHA-a3-GFP* and *pBZR1*:*BZR1-mCherry*. The co-IP assays confirmed the interaction between VHA-a3 and BZR1 (Figure 3A). Co-IP assays in *N. benthamiana* leaves also validated the interaction of BZR1 with VHA-a2 and VHA-a3 (Supplemental Figure 5B). To examine whether VHA-a2 and VHA-a3 directly interacted with BZR1, we performed *in vitro* pull-down assays using recombinant glutathione *S*-transferase (GST)-tagged BZR1 and maltose-binding protein (MBP)-tagged VHA-a2 and VHA-a3. GST-tagged BZR1, but not GST alone, pulled down *MBP-VHA-a2* and *MBP-VHA-a3* (Figure 3B). Fluorescence lifetime microscopy (FLIM) has also been used to detect protein–protein interactions *in vivo* by measuring fluorescence resonance energy transfer (FRET) (Long et al., 2017). Here, the fluorescence lifetime of VHA-a3-GFP was significantly reduced in root cells of 5-DAG seedlings harboring *pVHA-a3*:*VHA-a3-GFP* and *pBZR1*:*BZR1-mCherry* compared with those harboring *pVHA-a3*:*VHA-a3-GFP* alone (Figure 3C and 3D). BR treatment resulted in BZR1-mCherry entering the nucleus, and the abundance of cytoplasmic BZR1-mCherry was reduced, which led to a decrease in tonoplast-localized BZR1 protein (Figures 2D–2I and 3C). Because BR treatment causes separation between VHA-a2-GFP and BZR1-mCherry and between VHA-a3-GFP and BZR1-mCherry, fluorescence transfer from VHA-a3-GFP to BZR1-mCherry was reduced and the VHA-a3-GFP fluorescence lifetime was significantly increased compared with that in untreated seedlings (Figure 3C and 3D). The chance of interactions between VHA-a2 and tonoplast-localized BZR1 and between VHA-a3 and tonoplast-localized BZR1 was significantly reduced after BR treatment, further suggesting that the interactions between VHA-a2 and BZR1 and between VHA-a3 and BZR1 occur on the tonoplast.

V-ATPase is partially conserved across *Arabidopsis*, fruit flies (*Drosophila melanogaster*), mice (*Mus musculus*), humans (*Homo sapiens*), and yeast (*Saccharomyces cerevisiae*), especially over the transmembrane domain (Supplemental Figure 8) (Hiesinger et al., 2005; Marshansky et al., 2014). A study in *D. melanogaster* showed that two highly conserved amino acids in the first transmembrane region influence local intracellular protein trafficking (Hiesinger et al., 2005). Based on the above results of BZR1 trafficking, we speculated that these two amino acids (A427 in VHA-a3 and A428 in VHA-a2; G434 in VHA-a3 and G435 in VHA-a2), which are conserved among various species, are crucial for the interaction of VHA-a2 and VHA-a3 with BZR1. We transiently co-expressed *pUBQ10*:*VHA-a2-GFP*, *pUBQ10*:*VHAa2*$^{A428V+G435R}$*-GFP* (with mutations in the conserved amino acids), *pUBQ10*:*VHA-a3-GFP*, or *pUBQ10*:*VHA-a3*$^{A427V+G434R}$*-GFP* with *pBZR1*:*BZR1-mCherry* in *N. benthamiana* leaves and assessed the BZR1-mCherry fluorescence (Supplemental Figure 9A). When normal *VHA-a2* or *VHA-a3* was expressed in *N. benthamiana* leaves, BZR1-mCherry fluorescence was observed in the cytoplasm and nucleus, and BZR1-mCherry clearly co-localized with VHA-a2-GFP or VHA-a3-GFP on the tonoplast. When *VHA-a2*$^{A428V+G435R}$ or *VHA-a3*$^{A428V+G435R}$ was expressed in *N. benthamiana* leaves, levels of nuclear BZR1-mCherry significantly increased, whereas those of cytoplasmic BZR1-mCherry significantly decreased (Supplemental Figure 9A). We also examined *DWF4* transcript levels via qRT–PCR and BZR1 protein levels via nucleocytoplasmic separation in the co-transformed *N. benthamiana* leaves. Leaves expressing *VHA-a2*$^{A428V+G435R}$ or *VHA-a3*$^{A428V+G435R}$ had lower *DWF4* transcript levels than leaves expressing normal *VHA-a2* or *VHA-a3*, indicating higher BR signaling in leaves expressing *VHA-a2*$^{A428V+G435R}$ or *VHA-a3*$^{A428V+G435R}$ (Supplemental Figure 9B). Nucleocytoplasmic separation analysis also demonstrated that the abundance of nuclear-localized BZR1 was significantly higher in leaves expressing *VHA-a2*$^{A428V+G435R}$ or *VHA-a3*$^{A428V+G435R}$, whereas BZR1 was mainly localized in the cytoplasm in leaves expressing normal *VHA-a2* or *VHA-a3* (Supplemental Figure 9C and 9D). We also generated transgenic plants harboring *pVHA-a3*:*VHA-a3*$^{A427V+G434R}$*-GFP* in the Col and *vha2* backgrounds. 5-DAG-seedlings harboring *pVHA-a3*:*VHA-a3*$^{A427V+G434R}$*-GFP* in the *vha2* background had lower *CPD* and *DWF4* transcript levels than those in the Col background, indicating higher BR signaling in *pVHA-a3*:*VHA-a3*$^{A427V+G434R}$*-GFP vha2* seedlings (Figure 3E). We then examined the subcellular localization of BZR1 in *pVHA-a3*:*VHA-a3*$^{A427V+G434R}$*-GFP vha2* (Figure 3F). Immunoblot analysis revealed that *pVHA-a3*:*VHA-a3*$^{A427V+G434R}$*-GFP vha2* accumulated more unphosphorylated BZR1 in the nucleus compared with *pVHA-a3*:*VHA-a3*$^{A427V+G434R}$*-GFP* Col (Figure 3F and 3G); these results were similar to those in *vha2*, indicating that the two mutated residues are important for VHA-a2 and VHA-a3 functions. To further verify the role of these two conserved residues, we performed a pull-down assay using recombinant *MBP-VHA-a2*$^{A428V+G435R}$ and *MBP-VHA-a3*$^{A427V+G434R}$. We observed a significantly reduced interaction between BZR1 and VHA-a2$^{A428V+G435R}$ or VHA-a3$^{A427V+G434R}$ compared with the original VHA-a2 and VHA-a3 (Supplemental Figure 9E), demonstrating the crucial role of these amino acids in interactions of VHA-a2 and VHA-a3 with BZR1, as well as subsequent BZR1 localization.

BZR1 regulates the expression of *VHA-a2* and *VHA-a3* via a feedback loop

BR mediates plant development through the BR signal transduction pathway regulated by BZR/BES family members (Ryu et al., 2007; Sun et al., 2010). After BR signaling is activated, these transcription factors bind to the promoters of their target genes through NN-BRRE-core (NNCGTG), G-box (CACGTG), and E-box (CANNTG) motifs (Oh et al., 2012; Nosaki et al., 2018), leading to their up- or downregulation. Transcriptome profiling and chromatin immunoprecipitation (ChIP) microarray experiments showed that *VHA-a3* is a direct BZR1 target (Sun et al., 2010). We also confirmed that the transcript levels of *VHA-a2* and *VHA-a3* were significantly higher in *bzr1-1D* and significantly lower in *bri1-301* (Figure 4A). Based on these results, we hypothesized that BZR1 not only interacts with VHA-a2 and VHA-a3 but also activates the transcription of their corresponding genes.

To investigate the transcriptional regulation of *VHA-a2* and *VHA-a3*, we analyzed their promoters and identified several

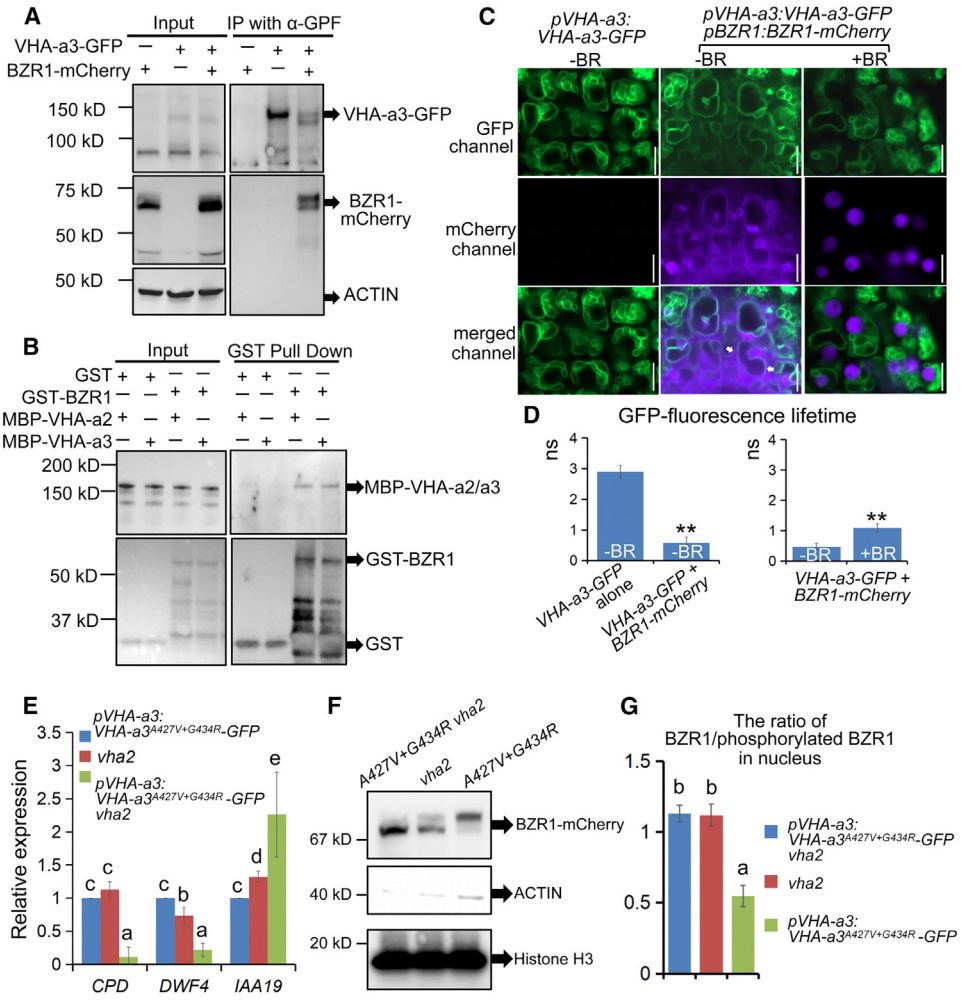

Figure 3. VHA-a2 and VHA-a3 interact with BZR1 through a domain conserved among multiple species.

(A) Co-immunoprecipitation (IP) assays demonstrated that BZR1-mCherry interacts with VHA-a3-GFP in 5-DAG light-grown seedlings harboring *pVHA-a3*:*VHA-a3-GFP* and *pBZR1*:*BZR1-mCherry*.

(B) *In vitro* pull-down assays demonstrated direct interactions between MBP-VHA-a2 and GST-BZR1 and between MBP-VHA-a3 and GST-BZR1.

(C) Confocal microscopy examination of the root elongation zone of seedlings harboring *pVHA-a3*:*VHA-a3-GFP* or *pVHA-a3*:*VHA-a3-GFP* + *pBZR1*:*BZR1-mCherry in vivo*. White arrows indicate the co-localization of the two proteins. Seedlings were treated with (+BR) or without (−BR) 1 μM eBL for 30 min before observation (n = 15). Scale bars represent 20 μm.

(D) Semi-quantitative analysis of fluorescence lifetimes in the root elongation zones of seedlings harboring *pVHA-a3*:*VHA-a3-GFP* or *pVHA-a3*:*VHA-a3-GFP* + *pBZR1*:*BZR1-mCherry* and seedlings harboring *pVHA-a3*:*VHA-a3-GFP* + *pBZR1*:*BZR1-mCherry* treated with (+BR) or without (−BR) BR *in vivo*. Bars represent the mean ± SD of three biological replicates (10 cells were measured separately for each biological replicate). Asterisks indicate significant differences (Student's *t*-test; $^{**}p < 0.01$).

(E) Transcript levels of *CPD*, *DWF4*, and *IAA19* in 5-DAG light-grown seedlings of *pVHA-a3*:*VHA-a3*$^{A427V+G434R}$*-GFP*, *vha2*, and *pVHA-a3*:*VHA-a3*$^{A427V+G434R}$*-GFP vha2*. Error bars represent CIs calculated from three biological replicates (each biological replicate was composed of three technical replicates) of each sample in the qRT–PCR assay. Lowercase letters indicate statistically significant differences among different materials (one-way ANOVA, $p < 0.05$).

(F) Nuclear protein separation analysis of 5-DAG light-grown seedlings of *pVHA-a3*:*VHA-a3*$^{A427V+G434R}$*-GFP BZR1-mCherry*, *vha2 BZR1-mCherry*, and *pVHA-a3*:*VHA-a3*$^{A427V+G434R}$*-GFP vha2 BZR1-mCherry* using an anti-mCherry antibody.

(G) Ratio of BZR1/phosphorylated BZR1 in **(F)**. Error bars represent the mean ± SD (n = 3). Lowercase letters indicate statistically significant differences among different materials (one-way ANOVA, $p < 0.05$).

NN-BRRE-core and E-box motifs (Figure 4B). We performed ChIP assays using three fragments harboring multiple NN-BRRE-core and E-box motifs of *VHA-a2* and *VHA-a3* (Figure 4B) and determined that BZR1 binds directly to these promoter regions (Figure 4C). Next, following a previously described method (Nosaki et al., 2018), we performed dual-luciferase (dual-LUC) assays using the firefly luciferase (*LUC*) reporter gene driven by] *VHA-a2* or *VHA-a3* promoters containing mutated NN-BRRE-core (NNCGTG to NNAAAA) and E-box (CANNTG to CAAAAA) motifs (Figure 4D). The dual-LUC assays indicated that BZR1 activates transcription of *VHA-a2* and *VHA-a3* (Figure 4E). Furthermore, *in vitro* eBL treatment increased BR signaling in *N. benthamiana* leaves and significantly enhanced BZR1 targeting to the *VHA-a2*

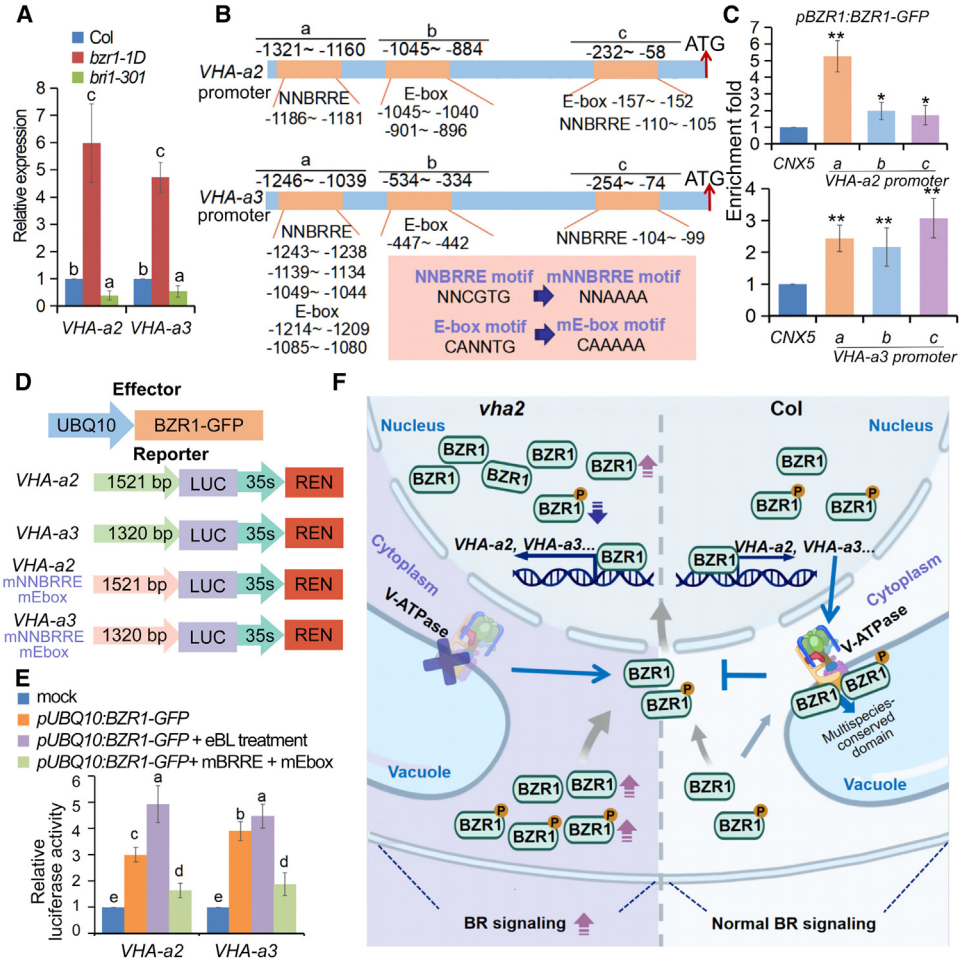

Figure 4. BZR1 binds directly to the NN-BRRE-core and E-box motifs in the *VHA-a2* and *VHA-a3* promoters.

(A) Transcript levels of *VHA-a2* and *VHA-a3* in 5-DAG light-grown seedlings of Col, *bzr1-1D*, and *bri1-301*. Error bars represent CIs calculated from three biological replicates (each biological replicate was composed of three technical replicates) fofor each sample in the qRT–PCR assay. Lowercase letters indicate statistically significant differences among different materials (one-way ANOVA, $p < 0.05$).

(B) Diagram of *VHA-a2* and *VHA-a3* promoter fragments and the specific locations of the NN-BRRE-core and E-box motifs. The adenine residue of the respective translation start codon (ATG) was assigned position +1; a, b, and c indicate the locations of amplicons used for the chromatin immunoprecipitation (ChIP)–qPCR assays shown in **(C)**.

(C) ChIP–qPCR assays using 7-DAG *pBZR1:BZR1-YFP* seedlings showed that BZR1 binds to the *VHA-a2* and *VHA-a3* promoters. Error bars represent CIs calculated from three biological replicates (each biological replicate was composed of three technical replicates) of each sample in the qRT–PCR assay. Asterisks indicate significant differences compared with the respective Col control (Student's *t*-test; $*p < 0.05$, $**p < 0.01$).

(D) Diagrams of effector and reporter constructs used in **(E)** (*VHA-a2*: −1521 bp to 0 bp; *VHA-a3*: −1320 bp to 0 bp). mNN-BRRE represents the mutated NN-BRRE-core motif (NNCGTG to NNAAAA), and mE-box represents the mutated E-box motif (CANNTG to CAAAAA).

(E) Dual-luciferase assays using the constructs in **(D)** indicate that BZR1 transcriptionally activates *VHA-a2* and *VHA-a3* by binding to the NN-BRRE-core and E-box motifs, and this transcriptional activation is induced by BR. Bars represent the mean ± SD of three biological replicates (each biological replicate is composed of 10 technical replicates). Lowercase letters indicate statistically significant differences among different materials (one-way ANOVA, $p < 0.05$).

(F) A schematic diagram illustrating the role of V-ATPase in BZR1 signaling. The VHA-a2 and VHA-a3 subunits of V-ATPase directly interact with BZR1 via a conserved domain and influence the total amount of BZR1 and the relative amount of nuclear-localized unphosphorylated BZR1. BZR1 directly binds to the *VHA-a2* and *VHA-a3* promoters and regulates *VHA-a2* and *VHA-a3* transcription. Thus, vacuole-localized V-ATPase and BZR1 may form a feedback loop to regulate the homeostasis of BR signaling in *Arabidopsis*.

and *VHA-a3* promoters, as shown by the higher relative LUC activity measured (Figure 4E); however, mutation of the NN-BRRE-core and E-box motifs significantly decreased *LUC* transcription, demonstrating that these two motifs are critical for BZR1 transcriptional regulation of *VHA-a2* and *VHA-a3* (Figure 4E). These results confirmed that BZR1 transcriptionally activates *VHA-a2* and *VHA-a3* by binding to the NN-BRRE-core and E-box motifs, and this regulation is induced by BR. Collectively, our results demonstrated that VHA-a2 and VHA-a3 interact directly with BZR1 and reduce unphosphorylated BZR1 in the nucleus. The reduction in nuclear unphosphorylated BZR1 in turn reduces *VHA-a2* and *VHA-a3* transcription, forming a feedback loop to maintain BR signaling homeostasis (Figure 4F).

DISCUSSION

Plant hormone function depends on the transport and localization of key proteins, which sometimes rely on regulation of the endomembrane system. The vacuole is essential to the plant endomembrane system, and the structure and function of the vacuole depend on the stability of solute concentrations across the tonoplast. Two tonoplast proton pumps (V-PPase and V-ATPase) maintain the proton-motive force for substance transport. V-PPase is a homodimer of a single polypeptide (Maeshima, 2000), and loss of function of V-PPase can be offset by raising the ATP/H-coupling rate and H^+-pumping activity of V-ATPase in *Arabidopsis* (Kriegel et al., 2015). AVP1 can rescue the V-ATPase deletion mutant *vph1* (*vacuolar pH1*) in yeast, but *AVP1* overexpression in *Arabidopsis* fails to rescue the *vha2* mutant phenotype (Pérez-Castiñeira et al., 2011; Coonrod et al., 2013; Kriegel et al., 2015). V-PPase also functions as a backup proton pump under ATP-limited conditions (Maeshima, 2000). We therefore focused on V-ATPase, given its apparently greater importance in *Arabidopsis*. VHA-a2 and VHA-a3 are tonoplast-localized isoforms of the integral membrane V-ATPase subunit VHA-a and have redundant functions with almost identical features (Krebs et al., 2010; Lupanga et al., 2020). VHA-a3 is more abundant than VHA-a2 at the tonoplast (Krebs et al., 2010; Lupanga et al., 2020). Thus, considering the stability of the transgenic process, VHA-a3 was used as the marker gene for stably transformed *Arabidopsis*. For transient transformation experiments in *N. benthamiana* and pull-down assays *in vitro*, we performed experiments on both VHA-a2 and VHA-a3 proteins, and the results for VHA-a2 and VHA-a3 were similar (Supplemental Figures 5, 6, and 9).

Several tonoplast proteins maintain vacuole morphology and integrity and thus regulate the localization of key proteins, including the receptor kinases BRI1 and BAK1, which are involved in BR signaling (Luo et al., 2015; Liu et al., 2018). Endocytic trafficking of the BRI1–BR complex in the *vha2* mutant is largely unchanged compared with that in Col (Luo et al., 2015). In this study, immunoblot analysis also showed that BRI1 and BAK1 levels did not differ significantly between *vha2* and Col seedlings (Supplemental Figure 3A). Furthermore, changing the vacuole structure alone is unlikely to result in the increased BR sensitivity observed in *vha2*. The *vps35 a-1 c-1* (*vacuolar protein sorting 35*), *vti11* (*vesicle transport v-snare 11*), and *pat2-2* (*protein affected trafficking 2-2*) mutants have abnormal vacuole structures, but their BR sensitivity is similar to that of Col (Sanmartín et al., 2007; Feraru et al., 2010; Munch et al., 2015). This finding indicates that the increased BR sensitivity of *vha2* is indeed caused by loss of VHA-a2 and VHA-a3 function, thus supporting our conclusion.

Our results revealed that VHA-a2 and VHA-a3 mediate BR signaling in *Arabidopsis*. Because immunoblot analysis could not detect BZR1 in vacuoles (probably targeted to the tonoplast) directly (this was too difficult, as we only could detect it in the cytoplasm), we used nuclear-localized unphosphorylated BZR1 to measure the level of BR signaling, following the approach of previous publications (Ryu et al., 2007; Qi et al., 2021). *vha2* shows increased BR sensitivity of root growth in light-grown seedlings, decreased sensitivity of BRZ for hypocotyl growth in dark-grown seedlings, reduced transcript levels of BR biosynthetic genes (He et al., 2005; Li and Deng, 2005; Sun et al., 2010), increased amounts of total BZR1 and nuclear-localized BZR1, and a higher BZR1/dephosphorylated BZR1 ratio than Col (Figures 1 and 2A–2F; Supplemental Figure 3), all of which indicate activated BR signaling in *vha2*. Overall plant growth is usually enhanced when BR signaling is moderately activated, but *vha2* had reduced growth (Figure 1G; Supplemental Figure 3D and 3E). There are two possible explanations for this phenomenon: (1) the deficiency in V-ATPase activity affects not only BR signaling but also other aspects of plant growth; (2) the BR signal in *vha2* is too high and somehow inhibits growth and development, probably because of feedback repression of BR biosynthesis genes. *vha2* partially rescued the growth status of *bri1-702* and *bin2*$^{+/-}$ (Figure 1G and Supplemental Figure 3G). *vha2 bzr1-1D* plants had curly roots, similar to eBL-treated WT seedlings (Supplemental Figure 3E), and *vha2 bzr1-1D* seedlings were less sensitive to BRZ treatment (Figure 1H), indicating higher BR signaling in *vha2 bzr1-1D* seedlings. The *vha2 bzr1-1D* mutant had poorer growth than its parents (*vha2* and *bzr1-1D*) (Figure 1G and Supplemental Figure 3E), suggesting that excessive BR signaling inhibited its growth. However, the BR-related phenotypes of *vha2 bzr1-1D* were more severe than those of the parents (qRT–PCR of BR biosynthesis genes and curly roots, Supplemental Figure 3E), suggesting that V-ATPase-mediated regulation of plant growth and development may not fully overlap with BR regulation but is likely to be involved in regulation of BZR1, thus affecting BR signaling. RNA-seq and qRT–PCR suggested that BR biosynthesis genes (e.g., *CPD*, *DWF4*) were downregulated in *vha2* (Figure 1B, 1E, and 1F), consistent with previously reported BR-signal-enhanced plants (in a BR-signal-enhanced mutant, *CPD* and *DWF4* were downregulated by BZR1 through negative feedback repression [Zhang et al., 2009; Sun et al., 2010; Oh et al., 2014]). RNA-seq also revealed that many up-and downregulated DEGs in *vha2* overlapped with genes reported to be induced or repressed by BR (Supplemental Figure 2), further confirming that BR signaling is high in *vha2*. We concluded that VHA-a2 and VHA-a3 regulate BR signaling by interacting with BZR1 and influencing its subcellular localization, although we could not exclude the possibility that VHA-a2 and VHA-a3 also affect BR content or other phenomena. In general, increased BR content leads to increased BR signaling, but enhanced BR signaling probably did not come from increased BR content. Although we focused on BR signaling in this study, BR content is also worth investigating in the future. BZR1 is an important transcription factor in the BR signal transduction pathway that shuttles between the nucleus and the cytoplasm. In this paper, we demonstrated that VHA-a2 and VHA-a3 regulate the nucleocytoplasmic localization of BZR1 and that BZR1 transcriptionally activates VHA-a2 and VHA-a3 BZR1 (Figure 4). This finding provides clues to the mechanism by which BZR1 localizes in the cytoplasm and enhances our understanding of the feedback regulatory pathway of BR. In addition, BR regulates the autophagic degradation pathway in plant cells. BES1, a member of the BZR/BES family, balances plant growth and survival through selective autophagy and ubiquitin-mediated protein degradation (Nolan et al., 2017). As a vacuole-related mutant, *vha2* displays an autophagy-associated premature senescence phenotype (Krebs et al., 2010; Jiang et al., 2020). Therefore, we could not exclude the possibility that the increased BZR1 levels in *vha2* might result from vacuole-related autophagic degradation, which is worth studying in future work.

Eukaryotic V-ATPases are the most complex nanomotors among rotary ATPases, and V-ATPases have acquired additional functions during evolution, particularly in substance transport (Parra and Kane, 1998; Marshansky et al., 2014). Our previous study revealed that VHA-a2, VHA-a3, and AVP1 mediate exocytosis and localization of the auxin efflux protein PIN-FORMED 1 (PIN1) (Jiang et al., 2020). Here, we also demonstrated that V-ATPase modulates nucleocytoplasmic localization of BZR1 and directly interacts with BZR1 at the tonoplast through the VHA-a2 and VHA-a3 subunits of V-ATPase in *Arabidopsis*. However, our fluorescence observations suggest that BZR1 is broadly distributed in the cytoplasm (similar to a previous report by Wang et al. [2021]), with only a portion of BZR1 proteins co-localizing with VHA-a2 and VHA-a3 (Figures 2G–2I and 3C; Supplemental Figure 5). These results suggest that the role of VHA-a2 and VHA-a3 might not cover all the regulatory mechanisms of BZR1 cytoplasmic localization. The mechanism of BZR1 cytoplasmic localization was not addressed in this study; it is still unclear and is worth investigating further in the future. Here, we measured the total amount of BZR1 protein by treatments with the protein synthesis inhibitor cycloheximide (CHX) and the proteasome inhibitor MG132. The results indicated that BZR1 protein biosynthesis was higher in *vha2* than in Col (Supplemental Figure 10). It appeared that the increased BZR1 protein levels were probably due to elevated transcript levels and protein biosynthesis. Our results demonstrate that VHA-a2 and VHA-a3 directly interact with BZR1, and both phosphorylated and dephosphorylated BZR1 interact with VHA-a2 and VHA-a3 (Figure 3A and Supplemental Figure 5B). Given the current results, we could not conclude that the interactions between VHA-a2/a3 and BZR1 are directly linked to the phosphorylation status of BZR1; neither VHA-a2 nor VHA-a3 affect the phosphorylation level of BZR1 by interacting with PP2A or GRF6 and GRF10. The detailed association between VHA-a2/a3 and PP2A/GRFs is worth investigating in future work. We also revealed that the V-ATPase–BZR1 interaction is modulated by a domain of VHA-a2 and VHA-a3 that is conserved among multiple species. Eukaryotic cells contain many organelles, including vacuoles, endosomes, lysosomes, and the Golgi apparatus. The transport, targeting, and membrane fusion of vesicles associated with these membrane-bound organelles depend on the regulation of V-ATPase (Marshansky et al., 2014). The a subunits of V-ATPase are critical for transport and targeting in mammals, *D. melanogaster*, and other organisms (Hiesinger et al., 2005; Yan et al., 2009). The conserved V-ATPase in the mammalian brain regulates the renin–angiotensin system related to blood pressure (Abbas et al., 2020). The conserved V-ATPase is localized to the *trans*-Golgi network/early endosome in *D. melanogaster*, and VHA-a affects the anterograde trafficking of secreted proteins. Two conserved amino acid sites in the VHA-a subunit of *D. melanogaster* are important for substance transport (Hiesinger et al., 2005), and these two sites also regulate BZR1 subcellular localization in *N. benthamiana* and *Arabidopsis* (Figure 3E–3G; Supplemental Figures 7 and 8), suggesting that the VHA-a subunit has a conserved function in substance transport among multiple species. Our results demonstrated that vacuole-localized V-ATPase affects intracellular protein transport in *Arabidopsis* through this conserved domain. Above all, our investigation indicates that VHA-a2 and VHA-a3 promote targeting of BZR1 to the tonoplast by interacting with BZR1, and this could be a regulatory mechanism for inhibiting transport of BZR1 to the nucleus. Our study describes a novel mechanism for the subcellular localization of the BZR1 protein and offers new insights into vacuole-mediated regulation of hormone signaling.

METHODS

Plant materials and growth conditions

All *Arabidopsis* plant materials in this research were in the Col-0 (*Arabidopsis thaliana* [L.] *Heynh*) ecotype background. Mutants used in this study have been described previously: *vha2*, obtained by crossing *vha-a2* (SALK_142642) with *vha-a3* (SALK_029786) from the Salk Institute for Biological Studies (Jiang et al., 2020); *bin2* (Li et al., 2001), *bzr1-1D* (He et al., 2002), *bri1-301*, *bri1-702* (Liu et al., 2018) (provided by Dr. Wen-Qiang Tang); the marker line *pBZR1:BZR1-YFP* (Wang et al., 2021) (provided by Dr. Wen-Qiang Tang); and *pSYP22:SYP22-RFP* (Shinoda et al., 2018) (provided by Dr. Jin-Xing Lin).

Seeds were surface sterilized with 2% NaClO for 5 min, washed four times with autoclaved water, and stratified at 4°C in darkness for 2 days. The seeds were positioned on half-strength Murashige and Skoog (1/2 MS) medium (Murashige and Skoog, 1962) containing 1.5% sucrose and 0.75% agar with a pH of 5.7–5.8 in a growth chamber (22°C, 16-h light/8-h dark cycle). At 7 DAG, seedlings were transferred to the soil under the same growth conditions (22°C, 16-h light/8-h dark cycle).

Plasmid construction and generation of transgenic plants

To generate the *pVHA-a3:VHA-a3-GFP* and *pBZR1:BZR1-mCherry* constructs, the promoters and gDNA fragments of *VHA-a3* and *BZR1* were amplified by PCR using genomic DNA of Col as templates and then cloned into the pHB vector (Biovector NTCC) digested by EcoRI and HindIII.

To generate the *pUBQ10:BZR1-mCherry*, *pUBQ10:VHA-a2-GFP*, *pUBQ10:VHA-a3-GFP*, *pUBQ10:BZR1S173A-YFP*, *pUBQ10:BZR1ΔPEST-YFP*, and *pUBQ10:BZR1TTTT-YFP* constructs, we first modified the PHB vector by replacing the 2× *35S* promoter with a *UBQ10* promoter. We then cloned the full-length coding sequences of *BZR1*, *VHA-a2*, and *VHA-a3* into the BamHI–HindIII sites of the modified PHB vector and cloned the coding sequences of *BZR1S173A*, *BZR1ΔPEST*, and *BZR1TTTT* from the Tang lab's constructs (Wang et al., 2021) into the BamHI–HindIII sites of the modified PHB vector.

To generate constructs for BiFC assays, the full-length coding sequences of *BZR1*, *GRF4*, *GRF6*, *GRF8*, *GRF10*, *PP2A-B′-α*, *PP2A-B′-β*, *VHA-a2*, and *VHA-a3* were cloned into the BamHI site of vectors pXY104 and pXY106, which encode the C- and N-terminal halves of YFP (cYFP and nYFP), respectively.

To generate *MBP-VHA-a2* and *MBP-VHA-a3* constructs, the full-length coding sequences of VHA-a2 and VHA-a3 were cloned into the BamHI–HindIII sites of pMal-c2X (New England Biolabs). The GST-BZR1 construct based on pET-GST (New England Biolabs) was described in our previous study (Zu et al., 2022). For construction of *pUBQ10:VHA-a2$^{A428V+G435R}$-GFP*, *pUBQ10:VHA-a3$^{A427V+G434R}$-GFP*, *pVHA-a3:VHA-a3$^{A427V+G434R}$-GFP*, *MBP-VHA-a2$^{A428V+G435R}$*, and *MBP-VHA-a3$^{A427V+G434R}$*, we introduced mutation sites in primers using the Fast Mutagenesis System (FM111-01, TransGen Biotech) according to the manufacturer's instructions.

To generate transgenic plants, the corresponding constructs were transformed into *Agrobacterium tumefaciens* (strain GV3101) and then into Col by the floral dip method (Clough and Bent, 1998). Primers used to generate the constructs are listed in Supplemental Table 1, and all constructs were confirmed by sequencing and alignment before being used in assays. Transgenic plants were selected on 1/2 MS medium containing specific antibiotics, and homozygous transgenic plants were used in assays.

In vitro chemical treatments

For BR sensitivity experiments with *Arabidopsis* seedlings, sterilized seeds were planted directly on 1/2 MS medium with 1.5% sucrose and 0.75% agar containing the indicated concentrations of eBL or BRZ. Two days

after vernalization, the light-grown seedlings were placed in a growth incubator (22°C, 16-h light/8-h dark cycle), and the dark-grown seedlings were wrapped in aluminum foil and then placed in the incubator. For immunoblotting and fluorescence observation experiments on BZR1 protein in light-grown seedlings, seedlings grown on 1/2 MS medium containing 0.2 μM BRZ (−BR) were used directly or after treatment with 1 μM eBL for 30 min (+BR), as described previously (Wang et al., 2021). For intact vacuole isolation assays and *in vitro* treatment of transiently transformed *N. benthamiana* leaves in dual-LUC assays, we cut the leaves, placed them in square dishes with liquid 1/2 MS medium containing 1 μM eBL or 1 μM BRZ, and shook them at a slow speed for 30 min.

For CHX and MG132 treatments, 7-DAG seedlings were first grown on 1/2 MS medium (Wang et al., 2021) with 0.2 μM BRZ, 1.5% sucrose, and 0.75% agar. The seedlings were then transferred to a new 1/2 MS medium with 0.2 μM BRZ and 200 μM CHX/50 μM MG132 for the indicated times, mounted in a drop of solution containing the same concentrations of BRZ and CHX/MG132 for confocal microscopy, or quick-frozen for immunoblotting.

RNA extraction and qRT–PCR assays

At 5 DAG, light-grown seedlings cultured in vertical square dishes were harvested, and total RNA was extracted using the RNAprep Pure Plant Kit (TIANGEN). cDNA was synthesized from 2 μg total RNA using the RevertAid First Strand cDNA Synthesis Kit (Thermo Fisher Scientific). qRT–PCR analyses were performed as described previously (Zhang et al., 2016). The thermal cycling conditions were as follows: 42 cycles of 95°C for 10 s, 56°C for 15 s, and 72°C for 20 s. Specific primers for each gene are listed in Supplemental Table 1. Results were normalized using *ACTIN2* as the endogenous control. Three biological replicates were analyzed for each experiment.

RNA-seq and data analysis

Samples for RNA-seq were collected from Col and *vha2*. Total RNA was isolated from 5-DAG seedlings. More than 100 mg of seedlings were collected with three biological replicates. Total RNA was isolated using the TRIzol reagent (Invitrogen Life Technologies) and then concentrated; its quality and integrity were determined using a NanoDrop spectrophotometer (Thermo Scientific). Next, mRNA with a poly(A) structure was enriched from total RNA using Oligo(dT) magnetic beads, and ion interruption was used to break the RNA into fragments of about 300 bp in length. The products were purified (AMPure XP system) and quantified using the Agilent high-sensitivity DNA assay on a Bioanalyzer 2100. First-strand cDNA was synthesized from the template RNA using 6-base random primers and reverse transcriptase, and second-strand cDNA was synthesized using the first-strand cDNA as the template. After RNA extraction, purification, and library construction, the libraries were subjected to paired-end next-generation sequencing on the Illumina platform. The quality-filtered reads were mapped to the Arabidopsis Information Resource (TAIR10) version of the *Arabidopsis* genome with HISAT2 v2.0.5, which is freely available at http://daehwankimlab.github.io/hisat2/. We used HTSeq (0.9.1) statistics to compare the read count values of each gene as the original expression of the gene, then used FPKM (fragments per kilobase per million mapped reads) to standardize the expression. Differentially expressed genes were identified with DESeq (1.30.0) using the criteria $|\log_2(\text{FoldChange})| > 1$ and $p < 0.05$. ClusterProfiler (3.4.4) was used to perform KEGG pathway enrichment analysis of the DEGs, focusing on significantly enriched pathways with p values <0.05.

Transmission electron microscopy

Cotyledon sections (1 mm^2) cut from 8-DAG *Arabidopsis* seedlings were vacuum-infiltrated and fixed overnight with 2.5% glutaraldehyde (Sigma, G5882) in 0.1 M PBS (pH 6.9) at 4°C. Samples were processed for electron microscopy as described by Guan et al. (2022). Observation and image capture were performed using a transmission electron microscope (Hitachi H-7650, Japan) at 80 kV.

Protein extraction and immunoblotting

For immunoblots of *Arabidopsis* and *N. benthamiana*, plant material (200 mg per sample) was ground into powder in liquid nitrogen, and total proteins were extracted using 500 μl of protein extraction buffer (100 mM Tris–HCl [pH 6.8], 20 mM dithiothreitol [DTT], 4% SDS, 100 mM NaCl, 0.1 mM bromophenol blue, 20% glycerol, 40 mM β-mercaptoethanol, 2 mM phenylmethylsulfonyl fluoride, 1× EDTA-free protease inhibitor cocktail). Samples in buffer were immediately boiled for 15 min and then centrifuged at 15 000 *g* for 5 min at 4°C. Proteins from the supernatant were used in subsequent immunoblotting assays.

For nucleocytoplasmic separation, plant materials (250 mg per sample) were ground into powder in liquid nitrogen and dissolved in 500 μl of extraction buffer A (20 mM Tris–HCl [pH 7.0], 250 mM sucrose, 25% glycerol, 20 mM KCl, 2 mM EDTA, 2.5 mM $MgCl_2$, 30 mM β-mercaptoethanol, 1× EDTA-free protease inhibitor cocktail, 0.7% Triton X-100). After incubation at 4°C with rotation for 30 min, samples were spun at 3000 *g* for 10 min at 4°C, and the supernatant was collected as the cytoplasmic extract. The pellets were washed four times with buffer A (5× pellet volume each time) and then spun at 3000 *g* for 20 min at 4°C. The white pellets were collected as the nuclear extract. The collected extracts were immediately added to an equal volume of protein extraction buffer, and protein extractions as were then carried out described above.

Immunoblotting was performed as described previously (Jiang et al., 2020). The antibodies used in this study were anti-GFP, anti-mCherry, anti-TUBULIN A, anti-ACTIN, anti-Histone H3, anti-MBP, and anti-GST from Abcam and anti-BZR1, anti-BES1, anti-BRI1, and anti-BAK1 from Abiocode.

Chromatin immunoprecipitation assays

ChIP was performed as described previously (Wang et al., 2020). In brief, 2 g of 7-DAG *pBZR1:BZR1-YFP* seedlings were treated as described above, crosslinked with formaldehyde, and used for chromatin isolation. The chromatin was sonicated for 5–10 min (10 s on and 10 s off) on ice and immunoprecipitated with anti-GFP beads. All primer sequences are shown in Supplemental Table 1. DNA fragments were quantified by qRT–PCR using specific primer sets (Supplemental Table 1). Col and immunoglobulin G were used as negative controls, and the values in Col were set to 1 after normalization for qPCR analysis.

Intact vacuole isolation assays

Vacuole isolation was performed as described previously (Robert et al., 2007). In brief, we extracted protoplasts from rosette leaves of 20-DAG *pBZR1:BZR1-YFP pSYP22:SYP22-RFP* plants grown under short-day (8-h light) conditions and then isolated vacuoles by osmotic and thermal disruption of protoplasts. For time-sensitive fluorescence observation, we did not perform vacuole enrichment through density gradient fractionation.

Transient expression in *Arabidopsis* mesophyll protoplasts

Arabidopsis protoplasts were extracted from rosette leaves of 20-DAG soil-grown seedlings under normal growth conditions (22°C, 16-h light/8-h dark cycle). Protoplast isolation and transient expression were performed as described by Yoo et al. (2007). In brief, constructs of BZR1-YFP, BZR1S173A-YFP, BZR1ΔPEST-YFP, and BZR1TTTT-YFP driven by the UBQ10 promoter were transfected into protoplasts and incubated for 16 h. For observation, 10 μl of the protoplast culture system was observed using the YFP channel, the chlorophyll autofluorescence channel, and the bright-field channel.

Dual-luciferase assays

Dual-LUC assays were performed using the Dual Luciferase Reporter Assay System (Promega) according to the manufacturer's instructions. LUC and *Renilla* (REN) activities were measured with a luminometer (GLOMAX 20/20, Promega), and the LUC/REN ratio was recorded.

In vitro pull-down assays

For *in vitro* pull-down assays, proteins were expressed in *Escherichia coli* (strain BL21) and purified. Three micrograms of purified recombinant bait proteins (GST-BZR1 and GST) and 5 μg of prey proteins (*MBP-VHA-a2* and *VHA-a3* or *MBP-VHA-a2*$^{A428V+G435R}$ and *MBP-VHA-a3*$^{A427V+G434R}$) were added to 1 ml of binding buffer (20 mM Tris–HCl [pH 8.0], 150 mM NaCl, 1 mM EDTA, 0.2% Triton X-100, 1× protease cocktail inhibitors) with 50 μl of glutathione agarose beads (GE Healthcare). After incubation for 3 h at 4°C, samples were washed four times with washing buffer (20 mM Tris–HCl [pH 8.0], 150 mM NaCl, 1 mM EDTA, 0.2% Triton X-100, 1× protease cocktail inhibitors). The pulled-down proteins were eluted with 2× SDS loading buffer and immediately boiled for 15 min. The input and eluted proteins were separated on 8% SDS–PAGE gels and immunoblotted with appropriate antibodies.

Co-immunoprecipitation assays

For *in vitro* co-IP assays, proteins were extracted from *N. benthamiana* epidermal cells transiently co-transformed with the constructs described above. For *in vivo* co-IP assays, proteins were extracted from 5-DAG *Arabidopsis* seedlings harboring two constructs with different fluorescent labels. Plant materials were ground into powder in liquid nitrogen and added to 1 ml of co-IP binding buffer (50 mM Tris–HCl [pH 8.0], 1 mM $MgCl_2$, 10 mM EDTA, 5 mM DTT, 500 mM sucrose, 100× protease cocktail inhibitors) with 50 μl of anti-GFP magnetic microbeads. After incubation for 3 h at 4°C, samples were washed four times with washing buffer (50 mM Tris–HCl [pH 8.0], 1 mM $MgCl_2$, 10 mM EDTA, 5 mM DTT, 500 mM sucrose, 100× protease cocktail inhibitors). Proteins were eluted with 2× SDS loading buffer and immediately boiled for 15 min. The input and eluted proteins were separated by 8% SDS–PAGE and immunoblotted with appropriate antibodies.

Bimolecular fluorescence complementation assays

We transformed constructs into *A. tumefaciens* (strain GV3101) and cultured the bacteria overnight in Luria–Bertani medium containing specific antibiotics. The samples were then resuspended to an OD_{600} of 1.0 in the infection solution (10 mM 2-(*N-morpholino)ethanesulfonic acid*, 10 mM $MgCl_2$, and 200 μM acetosyringone). The prepared suspensions were infiltrated into *N. benthamiana* leaves, and the plants were kept in darkness for 2 days. Fluorescent YFP signals were monitored with a Leica SP8 confocal microscope. *A. tumefaciens* harboring nYFP and cYFP constructs were mixed in equal ratios and infiltrated into *N. benthamiana* leaves after 2–4 h in darkness. After growth in darkness for 36–48 h, YFP signals in leaves were detected using a confocal microscope.

Confocal microscopy

To determine the fluorescence of *Arabidopsis* roots, 5-DAG vertically cultured seedlings were mounted in a drop of liquid 1/2 MS medium containing 10% glycerin. To study transient transformation of *N. benthamiana*, injection sites of *N. benthamiana* leaves were taken out and sealed with autoclaved water. Samples were observed with an Upright Laser Confocal Microscope (Nikon & Nikon Ni-E A1 HD25). The excitation and emission wavelengths were as follows: FB28, excitation at 395 nm and emission at 440–470 nm; GFP and YFP, excitation at 488 nm and emission at 505–550 nm; mCherry, excitation at 561 nm and emission at 575–620 nm. All samples were observed using the same parameters: confocal pinhole, 1.2 μm; excitation intensity, 5; HV, 30. Details of these methods have been described previously (Jiang et al., 2020).

FRET–FLIM assays

FRET–FLIM experiments were performed using an ISS Q2 laser scanning confocal microscope configured with a Q2 integrated confocal nanoimaging system and a fluorescence lifetime imaging system. Using VHA-a3-GFP as the donor and BZR1-mCherry as the acceptor, the GFP fluorescence lifetime of VHA-a3-GFP was measured as a negative control. All measurements were obtained from full-field images of vertically cultured 5-DAG *Arabidopsis* seedlings, and specific experimental methods were strictly followed as reported previously (Long et al., 2017). The fluorescence lifetimes of the donors were obtained with VistaVision software.

Accession numbers

Sequence data from this article can be found in the Arabidopsis Genome Initiative or GenBank/European Molecular Biology Laboratory databases under the following accession numbers: *VHA-a2* (AT2G21410), *VHA-a3* (AT4G39080), *BZR1* (AT1G75080), *BRI1* (AT4G39400), *BAK1* (AT4G33430), *BES1* (AT1G19350), *GRF4* (AT1G35160), *GRF6* (AT5G10450), *GRF8* (AT5G65430), *GRF10* (AT1G22300), *PP2A-B′-α* (AT5G03470), *PP2A-B′-β* (AT3G09880). The gene information involved in the RNA-seq data is labeled accordingly in Supplemental Dataset 1.

Quantification and statistical analysis

For all experiments, statistical analyses were carried out using Microsoft Office Excel software (Microsoft, USA). Two-tailed Student's *t*-tests were used to compare two groups. For comparisons of more than two groups, one-way ANOVA with Duncan's test was used ($p < 0.05$). Data are presented as the mean ± SD of at least three independent experiments, with *n* representing the number of biological replicates. For quantification, phenotypes were measured using ImageJ software (http://rsbweb.nih.gov/ij/download.html).

DATA AND CODE AVAILABILITY

The raw RNA-seq read data are deposited with links to BioProject PRJCA020369 at the China National Genomics Data Center (https://ngdc.cncb.ac.cn).

SUPPLEMENTAL INFORMATION

Supplemental information is available at *Molecular Plant Online*.

FUNDING

This research was supported by funding from the National Natural Science Foundation of China (32070342 and 32270339), the Agri-X Interdisciplinary Fund of Shanghai Jiao Tong University (Agri-X20200204), the Bio-X Interdisciplinary Fund of Shanghai Jiao Tong University (20CX-04), and the Scientific and Technological Innovation Funds of Shanghai Jiao Tong University (19X160020009).

AUTHOR CONTRIBUTIONS

W.-H.L. designed the study, supervised the project, analyzed data, organized results, modified the manuscript, and acquired funding. Y.-T.J. performed the experiments, analyzed data, organized results, and wrote the manuscript. L.-H.Y., J.-X.Z., X.-C.G., Y.-X.B., and Y.-C.W. helped to perform experiments and conducted association analysis. H.-W.X. provided advice for experimental design and manuscript organization.

ACKNOWLEDGMENTS

We thank Prof. Wen-Qiang Tang from Hebei Normal University for constructive discussion and providing seeds (*bri1-301*) and vectors (*pBZR1:BZR1-YFP*, *pBZR1:BZR1S173A-YFP*, *35S:BZR1ΔPEST-YFP*, *pBZR1:BZR1TTTT-YFP*), Prof. Jin-Xing Lin from Beijing Forestry University for providing seeds (*pSYP22:SYP22-RFP*), Prof. Hui-Qiong Zheng from CAS Center for Excellence in Molecular Plant Sciences—Institute of Plant Physiology and Ecology for technical guidance on ultra-thin sectioning, and Miss Yuan-Yuan Dong from Shanghai Jiao Tong

University for the methods of transient expression in *Arabidopsis* mesophyll protoplasts. We declare that we have no financial or personal relationships with other people or organizations that can inappropriately influence our work.

Received: May 27, 2023
Revised: September 29, 2023
Accepted: October 10, 2023
Published: October 12, 2023

REFERENCES

Abbas, Y.M., Wu, D., Bueler, S.A., Robinson, C.V., and Rubinstein, J.L. (2020). Structure of V-ATPase from the mammalian brain. Science **367**:1240–1246.

Burla, B., Pfrunder, S., Nagy, R., Francisco, R.M., Lee, Y., and Martinoia, E. (2013). Vacuolar Transport of Abscisic Acid Glucosyl Ester Is Mediated by ATP-Binding Cassette and Proton-Antiport Mechanisms in *Arabidopsis*. Plant Physiol. **163**:1446–1458.

Cipriano, D.J., Wang, Y., Bond, S., Hinton, A., Jefferies, K.C., Qi, J., and Forgac, M. (2008). Structure and regulation of the vacuolar ATPases. Biochim. Biophys. Acta **1777**:599–604.

Clough, S.J., and Bent, A.F. (1998). Floral dip: a simplified method for Agrobacterium-mediated transformation of *Arabidopsis thaliana*. Plant J. **16**:735–743.

Contrò, V., R Basile, J., and Proia, P. (2015). Sex steroid hormone receptors, their ligands, and nuclear and non-nuclear pathways. AIMS Mol. Sci. **2**:294–310.

Coonrod, E.M., Graham, L.A., Carpp, L.N., Carr, T.M., Stirrat, L., Bowers, K., Bryant, N.J., and Stevens, T.H. (2013). Homotypic vacuole fusion in yeast requires organelle acidification and not the V-ATPase membrane domain. Dev. Cell **27**:462–468.

Dettmer, J., Hong-Hermesdorf, A., Stierhof, Y.D., and Schumacher, K. (2006). Vacuolar H+-ATPase Activity Is Required for Endocytic and Secretory Trafficking in *Arabidopsis*. Plant Cell **18**:715–730.

Feraru, E., Paciorek, T., Feraru, M.I., Zwiewka, M., De Groodt, R., De Rycke, R., Kleine-Vehn, J., and Friml, J. (2010). The AP-3 β adaptin mediates the biogenesis and function of lytic vacuoles in *Arabidopsis*. Plant Cell **22**:2812–2824.

Goda, H., Sawa, S., Asami, T., Fujioka, S., Shimada, Y., and Yoshida, S. (2004). Comprehensive comparison of auxin-regulated and brassinosteroid-regulated genes in *Arabidopsis*. Plant Physiol. **134**:1555–1573.

Gaxiola, R.A., Palmgren, M.G., and Schumacher, K. (2007). Plant proton pumps. FEBS Lett. **581**:2204–2214.

Guan, B., Jiang, Y.-T., Lin, D.-L., Lin, W.-H., and Xue, H.-W. (2022). Phosphatidic acid suppresses autophagy through competitive inhibition by binding GAPC (glyceraldehyde-3-phosphate dehydrogenase) and PGK (phosphoglycerate kinase) proteins. Autophagy **18**:2656–2670.

He, J.X., Gendron, J.M., Yang, Y., Li, J., and Wang, Z.Y. (2002). The GSK3-like kinase BIN2 phosphorylates and destabilizes BZR1, a positive regulator of the brassinosteroid signaling pathway in *Arabidopsis*. Proc. Natl. Acad. Sci. USA **99**:10185–10190.

He, J.X., Gendron, J.M., Sun, Y., Gampala, S.S.L., Gendron, N., Sun, C.Q., and Wang, Z.Y. (2005). BZR1 Is a Transcriptional Repressor with Dual Roles in Brassinosteroid Homeostasis and Growth Responses. Science **307**:1634–1638.

Hedrich, R., Kurkdjian, A., Guern, J., and Flügge, U.I. (1989). Comparative studies on the electrical properties of the H+ translocating ATPase and pyrophosphatase of the vacuolar-lysosomal compartment. EMBO J. **8**:2835–2841.

Hiesinger, P.R., Fayyazuddin, A., Mehta, S.Q., Rosenmund, T., Schulze, K.L., Zhai, R.G., Verstreken, P., Cao, Y., Zhou, Y., Kunz, J., et al. (2005). The v-ATPase V0 subunit a1 is required for a late step in synaptic vesicle exocytosis in Drosophila. Cell **121**:607–620.

Ji, S., Han, Z., Kim, T.W., Wang, J., Cheng, W., Chang, J., Shi, S., Wang, J., Yang, M., Wang, Z.Y., et al. (2011). Structural insight into brassinosteroid perception by BRI1. Nature **474**:472–476.

Jiang, Y.T., Tang, R.J., Zhang, Y.J., Xue, H.W., Ferjani, A., Luan, S., and Lin, W.H. (2020). Two tonoplast proton pumps function in *Arabidopsis* embryo development. New Phytol. **225**:1606–1617.

Jiskrová, E., Novák, O., Pospíšilová, H., Holubová, K., Karády, M., Galuszka, P., Robert, S., and Frébort, I. (2016). Extra- and intracellular distribution of cytokinins in the leaves of monocots and dicots. Nat. Biotechnol. **33**:735–742.

Kinoshita, T., Caño-Delgado, A., Seto, H., Hiranuma, S., Fujioka, S., Yoshida, S., and Chory, J. (2005). Binding of brassinosteroids to the extracellular domain of plant receptor kinase BRI1. Nature **433**:167–171.

Krebs, M., Beyhl, D., Görlich, E., Al-Rasheid, K.A.S., Marten, I., Stierhof, Y.D., Hedrich, R., and Schumacher, K. (2010). *Arabidopsis* V-ATPase activity at the tonoplast is required for efficient nutrient storage but not for sodium accumulation. Proc. Natl. Acad. Sci. USA **107**:3251–3256.

Kriegel, A., Andrés, Z., Medzihradszky, A., Krüger, F., Scholl, S., Delang, S., Patir-Nebioglu, M.G., Gute, G., Yang, H., Murphy, A.S., et al. (2015). Job Sharing in the Endomembrane System: Vacuolar Acidification Requires the Combined Activity of V-ATPase and V-PPase. Plant Cell **27**:3383–3396.

Levin, E.R. (2015). Extranuclear steroid receptors are essential for steroid hormone actions. Annu. Rev. Med. **66**:271–280.

Li, J., Nam, K.H., Vafeados, D., and Chory, J. (2001). BIN2, a New Brassinosteroid-Insensitive Locus in *Arabidopsis*. Plant Physiol. **127**:14–22.

Li, L., and Deng, X.W. (2005). It runs in the family: regulation of brassinosteroid signaling by the BZR1-BES1 class of transcription factors. Trends Plant Sci. **10**:266–268.

Lin, W., Zhou, X., Tang, W., Takahashi, K., Pan, X., Dai, J., Ren, H., Zhu, X., Pan, S., Zheng, H., et al. (2021). TMK-based cell-surface auxin signalling activates cell-wall acidification. Nature **599**:278–282.

Liu, Q., Vain, T., Viotti, C., Doyle, S.M., Tarkowská, D., Novák, O., Zipfel, C., Sitbon, F., Robert, S., and Hofius, D. (2018). Vacuole Integrity Maintained by DUF300 Proteins Is Required for Brassinosteroid Signaling Regulation. Mol. Plant **11**:553–567.

Long, Y., Stahl, Y., Weidtkamp-Peters, S., Postma, M., Zhou, W., Goedhart, J., Sánchez-Pérez, M.I., Gadella, T.W.J., Simon, R., Scheres, B., et al. (2017). In vivo FRET-FLIM reveals cell-type-specific protein interactions in *Arabidopsis* roots. Nature **548**:97–102.

Luo, Y., Scholl, S., Doering, A., Zhang, Y., Irani, N.G., Rubbo, S.D., Neumetzler, L., Krishnamoorthy, P., Van Houtte, I., Mylle, E., et al. (2015). V-ATPase activity in the TGN/EE is required for exocytosis and recycling in *Arabidopsis*. Nat. Plants **1**:15094.

Lupanga, U., Röhrich, R., Askani, J., Hilmer, S., Kiefer, C., Krebs, M., Kanazawa, T., Ueda, T., and Schumacher, K. (2020). The *Arabidopsis* V-ATPase is localized to the TGN/EE via a seed plant-specific motif. Elife **9**:e60568.

Maeshima, M. (2000). Vacuolar H+-pyrophosphatase. Biochim. Biophys. Acta **1465**:37–51.

Marshansky, V., Rubinstein, J.L., and Grüber, G. (2014). Eukaryotic V-ATPase: Novel structural findings and functional insights. Biochim. Biophys. Acta **1837**:857–879.

Martinoia, E., Maeshima, M., and Neuhaus, H.E. (2007). Vacuolar transporters and their essential role in plant metabolism. J. Exp. Bot. **58**:83–102.

Marty, F. (1999). Plant Vacuoles. Plant Cell **11**:587–600.

Munch, D., Teh, O.K., Malinovsky, F.G., Liu, Q., Vetukuri, R.R., El Kasmi, F., Brodersen, P., Hara-Nishimura, I., Dangl, J.L., Petersen, M., et al. (2015). Retromer contributes to immunity-associated cell death in *Arabidopsis*. Plant Cell **27**:463–479.

Murashige, T., and Skoog, F. (1962). A revised medium for rapid growth and bioassays with tobacco tissue culture. Physiol. Plantarum **15**:473–497.

Nolan, T.M., Brennan, B., Yang, M., Chen, J., Zhang, M., Li, Z., Wang, X., Bassham, D.C., Walley, J., and Yin, Y. (2017). Selective Autophagy of BES1 Mediated by DSK2 Balances Plant Growth and Survival. Dev. Cell **41**:33–46.e7.

Nolan, T.M., Vukašinović, N., Hsu, C.W., Zhang, J., Vanhoutte, I., Shahan, R., Taylor, I.W., Greenstreet, L., Heitz, M., Afanassiev, A., et al. (2023). Brassinosteroid gene regulatory networks at cellular resolution in the *Arabidopsis* root. Science **31**:379.

Nosaki, S., Miyakawa, T., Xu, Y., Nakamura, A., Hirabayashi, K., Asami, T., Nakano, T., and Tanokura, M. (2018). Structural basis for brassinosteroid response by BIL1/BZR1. Nat. Plants **4**:771–776.

Oh, E., Zhu, J.Y., Ryu, H., Hwang, I., and Wang, Z.Y. (2014). TOPLESS mediates brassinosteroid-induced transcriptional repression through interaction with BZR1. Nat Commun **5**:4140.

Oh, E., Zhu, J.Y., and Wang, Z.Y. (2012). Interaction between BZR1 and PIF4 integrates brassinosteroid and environmental responses. Nat. Cell Biol. **14**:802–809.

Parra, K.J., and Kane, P.M. (1998). Reversible association between the V-1 and V-0 domains of yeast vacuolar H+-ATPase is an unconventional glucose-induced effect. Mol. Cell Biol. **18**:7064–7074.

Pérez-Castiñeira, J.R., Hernández, A., Drake, R., and Serrano, A. (2011). A plant proton-pumping inorganic pyrophosphatase functionally complements the vacuolar ATPase transport activity and confers bafilomycin resistance in yeast. Biochem. J. **437**:269–278.

Qi, G., Chen, H., Wang, D., Zheng, H., Tang, X., Guo, Z., Cheng, J., Chen, J., Wang, Y., Bai, M.Y., et al. (2021). The BZR1-EDS1 module regulates plant growth-defense coordination. Mol. Plant **14**:2072–2087.

Ranocha, P., Dima, O., Nagy, R., Felten, J., Corratgé-Faillie, C., Novák, O., Morreel, K., Lacombe, B., Martinez, Y., Pfrunder, S., et al. (2013). *Arabidopsis* WAT1 is a vacuolar auxin transport facilitator required for auxin homoeostasis. Nat. Commun. **4**:2625.

Robert, S., Zouhar, J., Carter, C., and Raikhel, N. (2007). Isolation of intact vacuoles from *Arabidopsis* rosette leaf-derived protoplasts. Nat. Protoc. **2**:259–262.

Ryu, H., Kim, K., Cho, H., Park, J., Choe, S., and Hwang, I. (2007). Nucleocytoplasmic Shuttling of BZR1 Mediated by Phosphorylation Is Essential in *Arabidopsis* Brassinosteroid Signaling. Plant Cell **19**:2749–2762.

Sanmartín, M., Ordóñez, A., Sohn, E.J., Robert, S., Sánchez-Serrano, J.J., Surpin, M.A., Raikhel, N.V., and Rojo, E. (2007). Divergent functions of VTI12 and VTI11 in trafficking to storage and lytic vacuoles in *Arabidopsis*. Proc. Natl. Acad. Sci. USA **104**:3645–3650.

Shinoda, H., Shannon, M., and Nagai, T. (2018). Fluorescent Proteins for Investigating Biological Events in Acidic Environments. Int. J. Mol. Sci. **19**, 1548.

Sun, Y., Fan, X.Y., Cao, D.M., Tang, W., He, K., Zhu, J.-Y., He, J.-X., Bai, M.Y., Zhu, S., Oh, E., et al. (2010). Integration of Brassinosteroid Signal Transduction with the Transcription Network for Plant Growth Regulation in *Arabidopsis*. Dev. Cell **19**:765–777.

Tang, W., Yuan, M., Wang, R., Yang, Y., Wang, C., Oses-Prieto, J.A., Kim, T.-W., Zhou, H.-W., Deng, Z., Gampala, S.S., et al. (2011). PP2A activates brassinosteroid-responsive gene expression and plant growth by dephosphorylating BZR1. Nat. Cell Biol. **13**:124–131.

Vasanthakumar, T., Bueler, S.A., Wu, D., Beilsten-Edmands, V., Robinson, C.V., and Rubinstein, J.L. (2019). Structural comparison of the vacuolar and Golgi V-ATPases from Saccharomyces cerevisiae. Proc. Natl. Acad. Sci. USA **116**:7272–7277.

Vukašinović, N., and Russinova, E. (2018). BRexit: Possible Brassinosteroid Export and Transport Routes. Trends Plant Sci. **285**.

Wang, L., Wang, B., Yu, H., Guo, H., Lin, T., Kou, L., Wang, A., Shao, N., Ma, H., Xiong, G., et al. (2020). Transcriptional regulation of strigolactone signalling in *Arabidopsis*. Nature **583**:277–281.

Wang, R., Liu, M., Yuan, M., Oses-Prieto, J.A., Cai, X., Sun, Y., Burlingame, A.L., Wang, Z.Y., and Tang, W. (2016). The Brassinosteroid-Activated BRI1 Receptor Kinase Is Switched off by Dephosphorylation Mediated by Cytoplasm-Localized PP2A B' Subunits. Mol. Plant **9**:148–157.

Wang, R., Wang, R., Liu, M., Yuan, W., Zhao, Z., Liu, X., Peng, Y., Yang, X., Sun, Y., and Tang, W. (2021). Nucleocytoplasmic trafficking and turnover mechanisms of BRASSINAZOLE RESISTANT1 in *Arabidopsis thaliana*. Proc. Natl. Acad. Sci. USA **118**, e2101838118.

Wang, X., and Chory, J. (2006). Brassinosteroids Regulate Dissociation of BKI1, a Negative Regulator of BRI1 Signaling, from the Plasma Membrane. Science **313**:1118–1122.

Wang, X., Li, X., Meisenhelder, J., Hunter, T., Yoshida, S., Asami, T., and Chory, J. (2005). Autoregulation and Homodimerization Are Involved in the Activation of the Plant Steroid Receptor. Dev. Cell **8**:855–865.

Yan, Y., Denef, N., and Schüpbach, T. (2009). The Vacuolar Proton Pump, V-ATPase, Is Required for Notch Signaling and Endosomal Trafficking in Drosophila. Dev. Cell **17**:387–402.

Yoo, S.D., Cho, Y.H., and Sheen, J. (2007). *Arabidopsis* mesophyll protoplasts: a versatile cell system for transient gene expression analysis. Nat Protoc **2**:1565–1572. https://doi.org/10.1038/nprot.2007.199.

Yu, Z., Ma, J., Zhang, M., Li, X., Sun, Y., Zhang, M., and Ding, Z. (2023). Auxin promotes hypocotyl elongation by enhancing BZR1 nuclear accumulation in *Arabidopsis*. Sci. Adv. **9**, eade2493.

Zhang, D., Tan, W., Yang, F., Han, Q., Deng, X., Guo, H., Liu, B., Yin, Y., and Lin, H. (2021). A BIN2-GLK1 Signaling Module Integrates Brassinosteroid and Light Signaling to Repress Chloroplast Development in the Dark. Dev. Cell **56**:310–324.e7.

Zhang, Y., Zhang, Y.J., Yang, B.J., Yu, X.X., Wang, D., Zu, S.H., Xue, H.W., and Lin, W.H. (2016). Functional characterization of GmBZL2 (AtBZR1 like gene) reveals the conserved BR signaling regulation in Glycine max. Sci. Rep. **6**, 31134.

Zhao, J., Benlekbir, S., and Rubinstein, J.L. (2015). Electron cryomicroscopy observation of rotational states in a eukaryotic V-ATPase. Nature **521**:241–245.

Zu, S.H., Jiang, Y.T., Chang, J.H., Zhang, Y.J., Xue, H.W., and Lin, W.H. (2022). Interaction of brassinosteroid and cytokinin promotes ovule initiation and increases seed number per silique in *Arabidopsis*. J. Integr. Plant Biol. **64**:702–716.

Zhang, S., Cai, Z., and Wang, X. (2009). The primary signaling outputs of brassinosteroids are regulated by abscisic acid signaling. Proc Natl Acad Sci U S A **106**:4543–4548.